S-wave velocity structure of the Sichuan-Yunnan region, China: implications for extrusion of Tibet Plateau and seismic activities

Haoyu Tian[1], Chuansong He[1]*, M. Santosh[2,3]

[1]Institute of Geophysics, China Earthquake Administration, Beijing 100081, China

[2]School of Earth Sciences and Resources, China University of Geosciences Beijing, Beijing 100083, China

[3]Department of Earth Science, University of Adelaide, Adelaide SA 5005, Australia

Abstract: The Sichuan-Yunnan region is located at the intersection between the South China Block, the Indian plate and the Tibet Plateau and is crisscrossed with deep and large faults and is characterized by strong seismic activities. Here we employ one-year continuous waveforms of the vertical

[1] Correspondence author: hechuansong@aliyun.com

component of 89 broadband seismic stations in this region to evaluate the velocity structure and its implications.

Through single station data preprocessing, cross-correlation calculation, stacking, group velocity dispersion measurement and quality evaluation, the group velocity dispersion curves of Rayleigh waves for the different periods were obtained. We then use the surface wave tomography method to obtain the Rayleigh wave group velocity distribution of 9-40s in this area. Finally, the S-wave velocity structure in the depth range of 0-60 km in the study area is obtained by pure path dispersion inversion. The results show that the surface layer or the top of the upper crust in the Sichuan Basin is characterized by low velocity due to the influence of the sedimentary strata, whereas the middle and lower crust of the Sichuan Basin shows high velocity structure. The Sichuan-Yunnan diamond-shaped block (SYDB) shows a high-velocity structure in the middle crust, , and a low velocity in the lower crust. The seismic activities are mainly concentrated at the western part of the region, with the earthquakes distributed at the boundary between the low- and high-velocity structures, as well as the adjacent region, which we correlate with the extrusion of the Tibet Plateau.

Key words: Noise tomography, Rayleigh surface wave, S-wave velocity, Crustal structure, Sichuan-Yunnan region.

1. Introduction

The Sichuan-Yunnan region of mainland China (99°E-109°E , 20°N-33°N) (Fig. 1) forms part of the southeastern margin of the Indo-Eurasian plate collision zone, as well as a turning point of the Tethyan-Himalayan orogenic system (Kan et al., 1977; Zhong et al., 1998; Deng et al., 2002). The region is located at the intersection between the South China Block, the Indian plate and the Tibet Plateau and is crisscrossed with deep and large faults, as represented by the Xiaojiang, Honghe, Lijiang-Ninglang, Anning River-Zemu River fault, Longmen Mountain and Maitreya-Shizong fault (Xu et al., 2003). This region also covers the central and southern domain of the North-South Seismic Belt, and is characterized by strong seismic activities (Li, 1993; Su et al., 2004; Zheng et al., 2012).

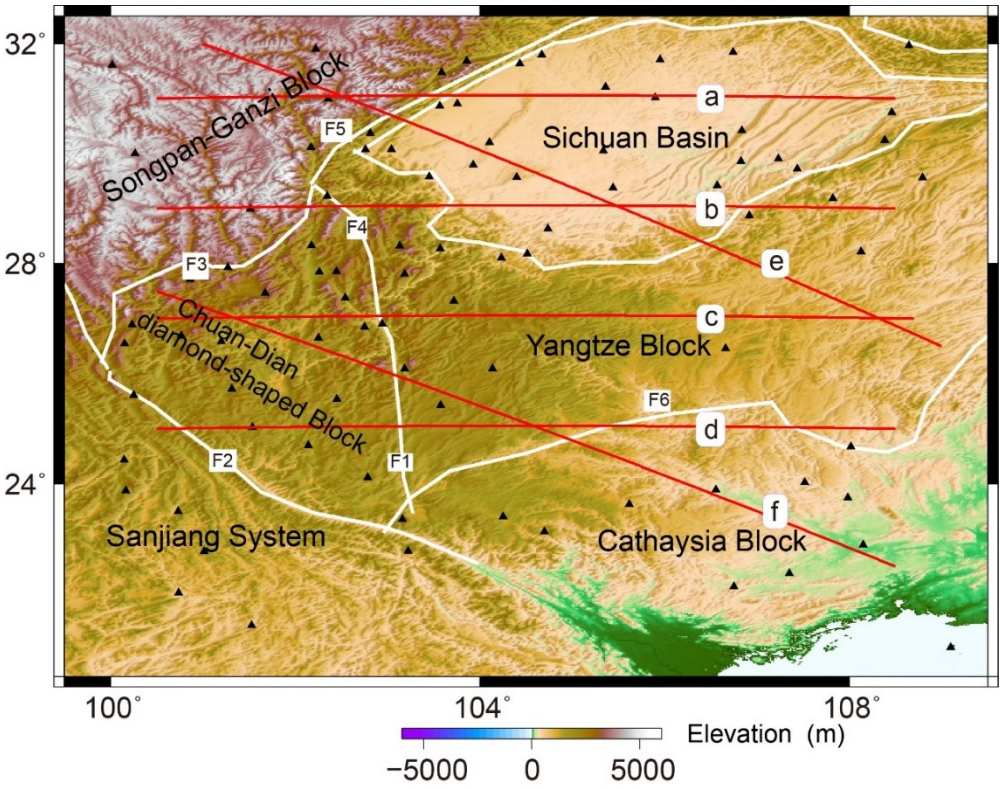

Fig. 1. Tectonic framework of the study area. The thick black lines show the boundaries of the various crustal blocks and basins. F1: Xiaojiang fault; F2: Honghe fault; F3: Lijiang-Ninglang fault; F4: Anning River-Zemu River fault; F5: Longmen Mountain fault; F6: Maitreya-Shizong fault. The black triangles are the locations of the seismic stations used in this study. Red lines: S-wave velocity profiles.

The unique geological and tectonic setting of this region, and earthquake-prone feature has attracted several studies to explore the deep features including seismic sounding (Hu et al., 1986 ; Wang et al.,

2014) , magnetotelluric sounding (Bai et al., 2010; Shen et al., 2015), body wave tomography (Liu et al., 1989; Wang et al., 2002; Huang et al., 2003; Xu et al., 2013; Lei et al., 2014), surface wave and noise tomography (Yao et al., 2006; Zhou et al., 2012; Zheng et al., 2015; Fan et al., 2015 ; Zheng et al., 2017), receiver function (Wu et al., 2001; Xu et al., 2007; Li et al., 2009; Xu et al, 2009; Wang et al., 2017; Hu et al., 2017) and surface wave and receiver function joint inversion (Bao et al., 2015).

Liu et al. (1989) noted that the velocity structure of the crust and upper mantle in the Sichuan-Yunnan region has obvious lateral heterogeneity based on teleseismic P-wave tomography. Wu et al. (2001) showed that the crust thickness in Yunnan area gradually decreases from northwest to southeast and the S-wave velocity structure is characterized by strong lateral inhomogeneity based on teleseismic receiver function inversion. Wang et al. (2002) employed P-wave and S-wave tomography and identified that the velocity anomalies of the lower crust and upper mantle are controlled by the faults. Huang et al. (2003) show that the velocity structure has obviously lateral heterogeneity in the Sichuan-Yunnan region by using the Pn tomography. Jiang et al. (2012) proposed that there is a significant difference in the crustal structure between the Sichuan Basin and the Songpan-Ganzi Block by using the Bouguer gravity data. Wang et al. (2014) used seismic

sounding to obtain a two-dimensional crustal structure of the region where the eastern side of the Red River Fault shows low velocity structure. Based on Pn tomography, Lei et al. (2014) imaged a high velocity anomaly in the Sichuan Basin area and an obvious low velocity anomaly zone from the Songpan-Ganzi Block to the SYDB. Bao et al. (2015) employed a joint inversion of the surface wave and receiving function and suggested a dramatic lateral change in the crustal S-wave velocity.

On the other hand, advances in seismic tomography has enabled high-resolution seismic imaging, with a direct cross-correlation of the continuous background noise of two stations (Lobkis and Weaver, 2001; Campillo and Paul, 2003; Shapiro et al., 2005; Yao et al., 2006; Bensen et al., 2007; Fang et al., 2009). Compared with traditional tomographic technique, noise imaging technology does not depend on the azimuth distribution of natural earthquakes, and moreover, seismic ray coverage is denser and more reasonable due to the increase of broadband seismic stations (Lu et al., 2014). This approach greatly improves the resolution of shallow crust due to an increase in the short-period dispersion data. Using this technique, Zheng et al. (2015) indicated there is a low-velocity layer in the middle and lower crust of the southeastern margin of the Tibet Plateau. Fan et al. (2015) revealed the lateral variation of sedimentary layer thickness in the Sichuan Basin. Zheng et al. (2012) defined the lateral heterogeneity of the crust and

the uplifted basement in the Sichuan Basin. Yao et al. (2006, 2008) suggested that the high and low velocity anomalies in this region are divided by some major fault zones.

In this study, using the data recorded by the China seismic network, we imaged the three-dimensional high-resolution velocity structure of the crust and upper mantle in the Sichuan-Yunnan area by using the noise tomographic technique. Our results provide new evidence on the terrane deformation, material migration, and seismic activities.

2. Data and method

2.1. Data and processing

We collected the continuous vertical-component seismic data recorded by 89 stations from Data Management Centre of China National Seismic Network from December 2016 to December 2017 (Zheng et al., 2009).

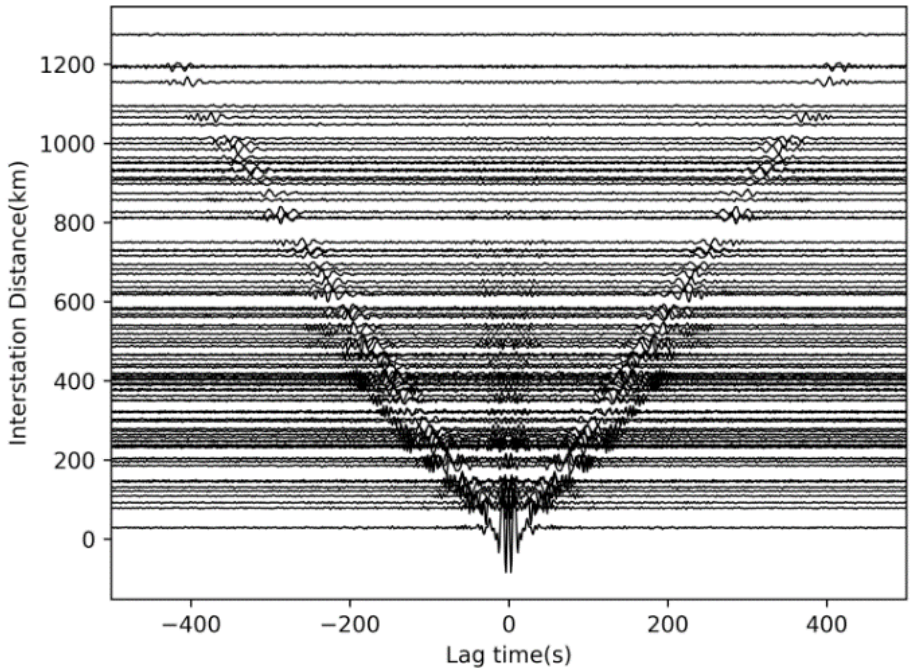

Fig. 2. The correlation of one-year data from the SCZJG seismic station related to other seismic stations with the period from 5 to 50 s.

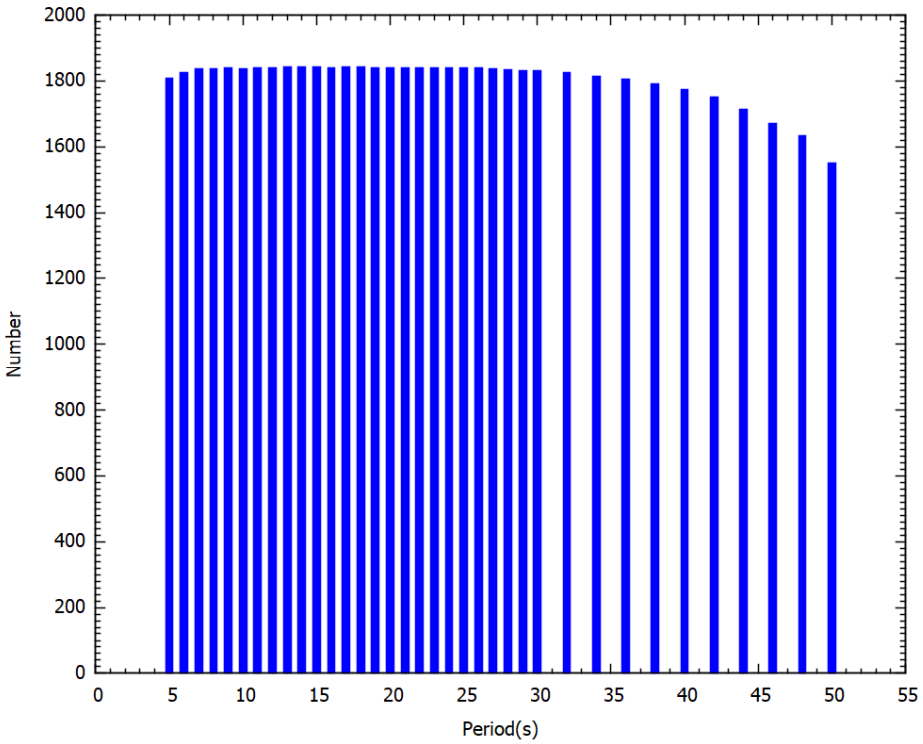

Fig. 3. The number of group velocity dispersion curves at different periods.

We adopted the data processing procedures following the method of Bensen et al. (2007) and Fang et al. (2009). Data are processed one day at a time for each station after being decimated to 1 Hz. Other parts involved instrument response removal, clock synchronization, time-domain normalization, bandpass filtering (4−50 s period), and spectral whitening. Following this, the day-long waveform at each station is correlated with other seismic stations and the daily results are stacked to produce the final cross-correlation results.

The resulting cross-correlations contain surface wave signals coming from

opposite directions along the path linking the stations. The cross-correlations are often asymmetrical due to the inhomogeneous distribution of ambient noise sources. To simplify data analysis and enhance the signal-to-noise ratio (SNR) of the surface waves, we separated each cross-correlation into positive and negative lag components and then added the two components to form the so-called symmetric component. The following analysis was done on the symmetric signals exclusively.

We use the CPS (Computer Programs in Seismology) software developed by Herrmann and manually picked up the group velocity dispersion curve based on the multiple filtering technology to (Dziewonski et al., 1969; Levshin et al., 1992 , Herrmann, 1973). If there are n stations, then the empirical Green's function on n(n-1)/2 paths can be calculated. In order to ensure reliable results, a quality control of the dispersion curve was carried out.

An empirical Green's function is accepted if its signal to noise ratio is greater than 10 and the inter-station distance is at least 3 times of wavelength at a given period (Yao et al., 2006; Bensen et al., 2007). Furthermore, we excluded paths that are shorter than 120 km because of the lack of adequate condition related to 3 times of the wavelength. Finally, a total of 1883 dispersion curves of the station pairs meeting the above requirements were

extracted from the 3916 Rayleigh wave waveform data (Fig. 2). We show in Fig. 3 the number of ray paths used for surface wave imaging at different periods, and confirm that the number of rays in most periods is relatively uniform.

2.2. Rayleigh wave velocity and S-wave velocity inversion

For the surface wave tomography, a generalized 2-D-linear inversion procedure developed by Ditmar and Yanovskaya (1987) and Yanovskaya and Ditmar (1990) was applied to construct the group velocity inversion, which is a generalization to 2-D inferred from the classical 1-D method of Backus and Gilbert (1968). In this study, we designed a 0.5° × 0.5° grid lateral. The damping parameter (α) controls the trade-off between the fit to the data and the smoothness of the resulting group velocity maps. We use the value of α = 0.2, which yields relatively smooth maps with small fit error.

From the Rayleigh wave group velocity obtained by the above inversion approach, we extracted the dispersion curves of group velocity at each grid node. We then inverted for the 1-D shear wave velocity structure under each grid node following the method of Herrmann and Ammon (2004). The velocities in between the nodes are interpolated linearly. In this way, a 3-D shear wave velocity structure was constructed (Fig. 4).

The initial model has a constant shear-wave velocity of 4.48 km/s from the surface to 90 km depth that is divided into 2 km layers. By starting with an overestimated velocity model, we ensured that no artificial low-velocity zone or layer boundary was introduced as a consequence of the nonlinear of the inversion. A fixed Vp/Vs ratio of 1.732 was used and the density was calculated from the P-wave velocity (Zanjani et al., 2019).

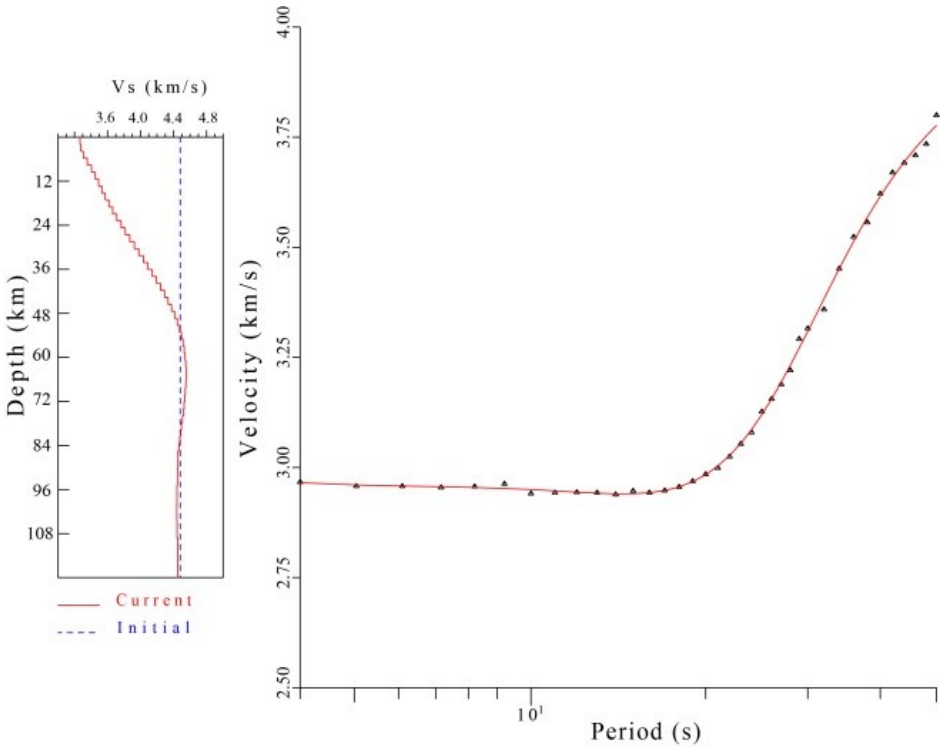

Fig. 4. The node (107°E, 22.5°N) as an example to illustrate the process of inverting the S-wave velocity from the dispersion curve. The black triangles in the right panel represent the group velocity observation dispersion. The red solid line represents the theoretical group velocity dispersion generated by the final S-wave velocity model obtained from the inversion. The blue dashed line

in the left panel represents the initial velocity model, whereas the red solid line represents the final S-wave velocity model obtained by the inversion.

3. Resolution analysis and results

3.1. Resolution analysis

In general, seismic tomography uses the checkerboard resolution test (CRT) to analyze the resolution and estimate the error of the results. However, Leveque et al. (1993) pointed out that the CRT used to analysis resolution may result in error. Yanovskaya (1997, 1998) used the mean scale and stretch of the mean area to estimate the imaging resolution, and the resolution of tomographic results is calculated based on the ray density and the ray azimuth distribution.

Fig. 5 represents the resolution of each period. The resolution radius distribution shows that the minimum resolution radius can reach within 50 km, whereas for most research areas, the resolution core radius can still reach 200 km. In this region, the obtained spatial average resolution radius is between 0 and 200 km, and the resolution radius is completely within the smooth radius allowed by the model parameters. According to the results of

the resolution detection, we consider that the inversion results of most areas in our study are relatively reliable.

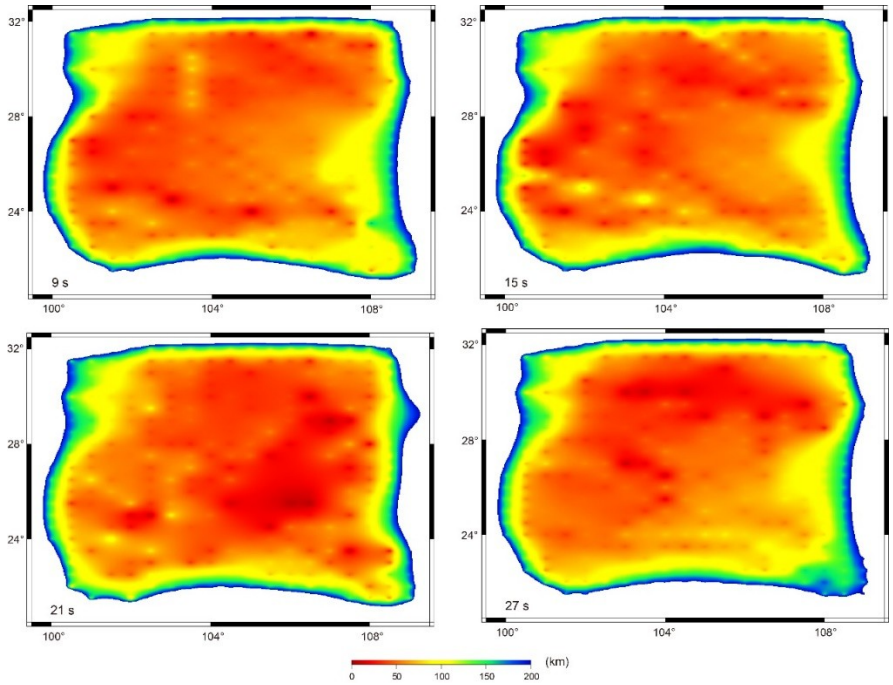

Fig. 5. The spatial average resolution radius distribution of different periods. The color scale at the bottom shows the resolution radius value.

3.2. Rayleigh wave velocity

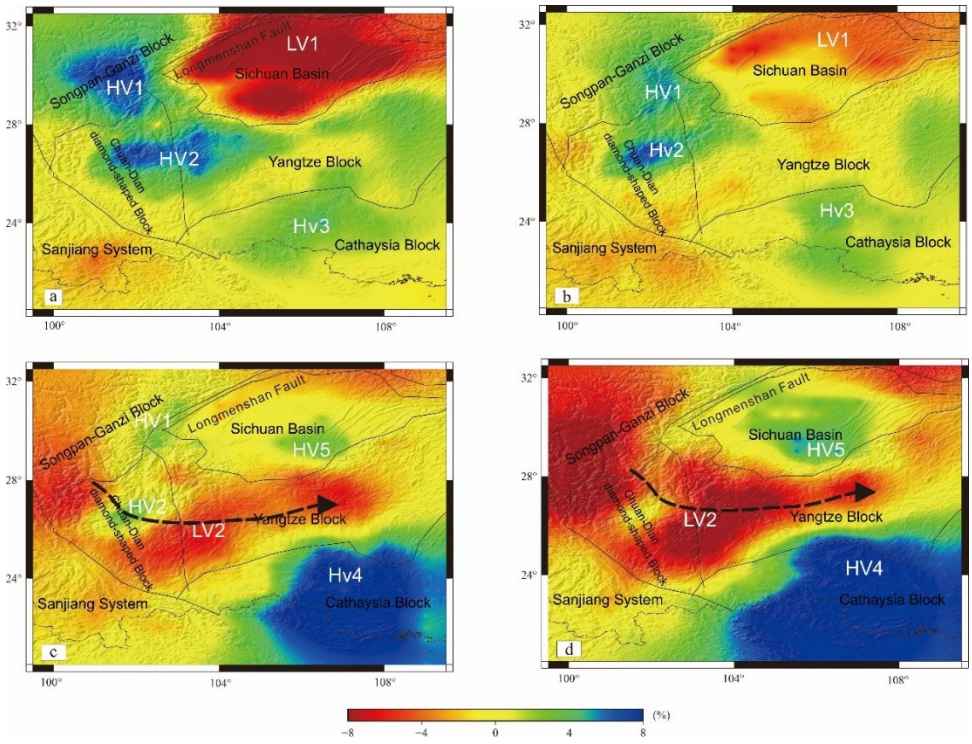

Fig. 6. Rayleigh wave group velocity in the different periods obtained by inversion of noise tomography. The corresponding periods: 9 s (a), 21 s (b), 25 s (c) and 38 s (d). The thick black lines represent the boundaries of the major geological/tectonic units. Black dotted lines and arrows in the c and d is the eastward channel flow.

The group velocity of a certain period is most sensitive to the shear wave velocity of 1/3 wavelength (Lin et al., 2007; Yang et al., 2007), and the group velocity distribution of the different periods represents the structural differences at different depths. According to the characteristics of the group velocity distribution of each period, we selected representative four-period group velocity for discussion (Fig. 6). The Rayleigh wave group velocity with T=9 s mainly reflects the velocity structure of the upper crust or the shallow

part of the crust (Fig. 6 a). The Sichuan Basin shows obvious low-velocity anomaly (Fig. 6 a, LV1) in the region, which is significantly affected by the sedimentary strata. Xie et al. (2013) also imaged a low-velocity anomaly from Rayleigh and Love wave phase speed at 10s in the Sichuan Basin. The Songpan-Ganzi Block, the northern part of the SYDB, the Cathaysia Bock, and the Yangtze Block mostly show high-velocity structure (Fig. 6 a, HV1, HV2 and HV3).

The Rayleigh wave group velocity with T=21 s mainly reflects the velocity structure of the middle crust (Fig. 6 b). The Sichuan Basin exhibits low-velocity structure (Fig. 6 b, LV1), with a relatively high Rayleigh wave group velocity in the center of the basin, which reflects the non-uniform feature of the basin. The Songpan Ganzi Block, the northern part of the SYDB and the Cathaysia Block all exhibit high velocity structure (Fig. 6 b, HV1, HV2 and HV3). The Rayleigh wave group velocity with meddle and long periods (25-38 s) mainly reflects the velocity structure from the lower crust to the top of the upper mantle (Fig. 6 c and d). At these periods, high-velocity structure (Fig. 6 c and d, HV4 and HV5) can be clearly seen in the Sichuan basin and the Cathaysia Block, whereas the southern part of the SYDB and most of the Yangtze Block are characterized by low-velocity structure (Fig. 6 c and d, LV2).

3.3. S-wave velocity structure

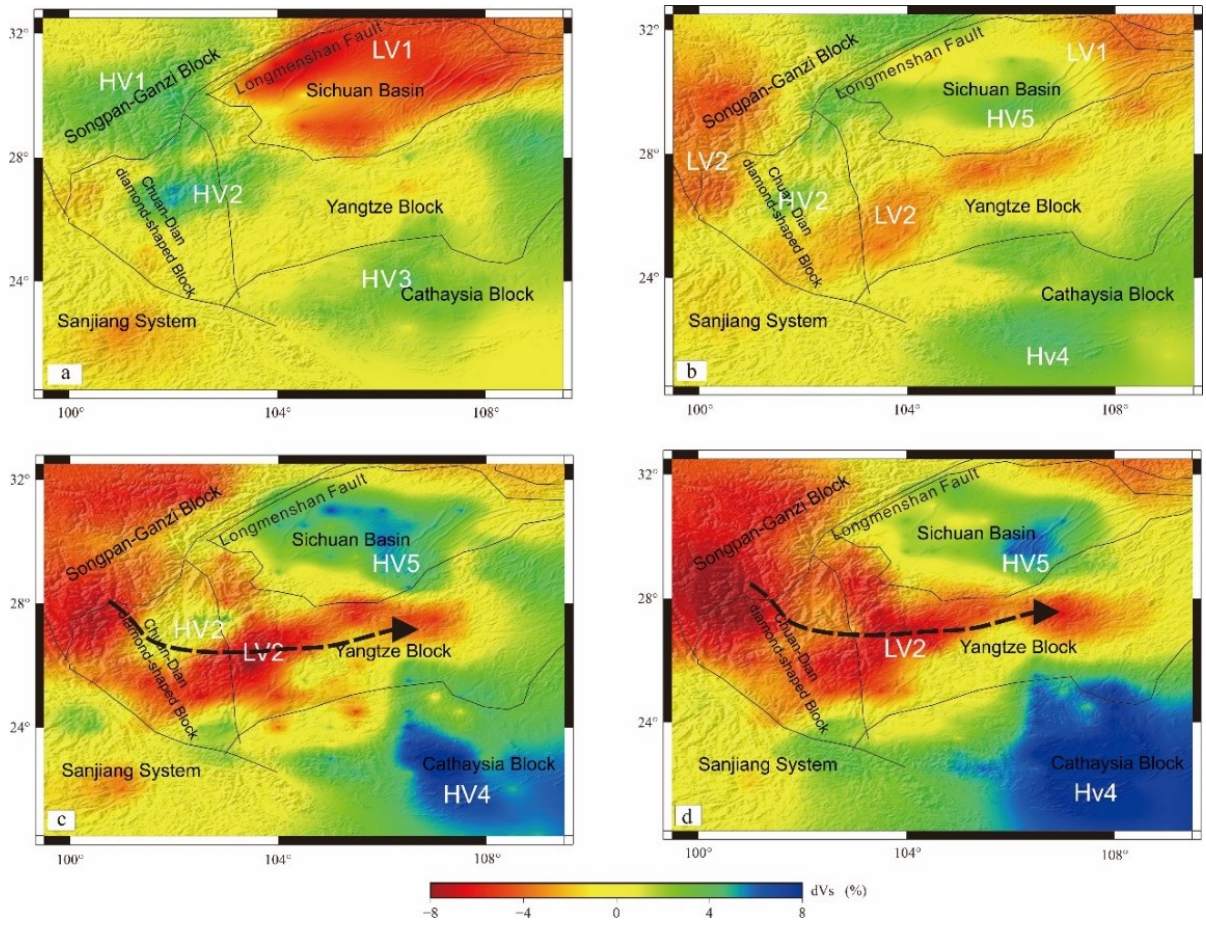

Fig. 7. S-wave velocity at different depths, a: 10 km, b: 20 km, c: 30 km and d: 46 km. The thick black lines mark the boundaries of the major geological/tectonic units. Black dotted lines and arrow represent the suggested eastward channel flow.

According to the 1-D shear wave velocity structure of each grid node obtained in this study, we construct a 3-D shear wave velocity structure ranging from a depth of 0 km to a depth 60 km in this area (Fig. 7). At the depth of 10 km (Fig. 7a), the Songpan-Ganzi Block, the northern part of the

SYRB, the Cathaysia Block and the eastern part of the Yangtze Block exhibit high-velocity anomalies (Fig. 7a, HV1, HV2 and HV3), whereas the Sichuan Basin exhibits low-velocity structure (LV1), which may be from the influence of the sedimentary strata. The Longmen Mountain fault zone is located on the boundary between the high-velocity (west) and the low-velocity (east) anomalies.

At the depth of the 20 km (Fig. 7 b), the Sichuan Basin and the Cathaysia Block shows high-velocity structures (Fig. 7 b, HV4 and HV5), whereas the Songpan-Garzi Block, the SYSB and the Yangtze Block are characterized by low-velocity structure (Fig. 7 b, LV2). Chen et al. (2014) revealed a low-velocity anomaly using the ambient noise adjoint tomography, which is similar to our LV2. At the depth of the 30 km-46 km, the Sichuan Basin and the Cathaysia Block shows high-velocity structures (Fig. 7 c and d, HV4 and HV5), whereas the Songpan-Garzi Block, the SYDB and the Yangtze Block have low-velocity structure (Fig. 7 c and d, LV2).

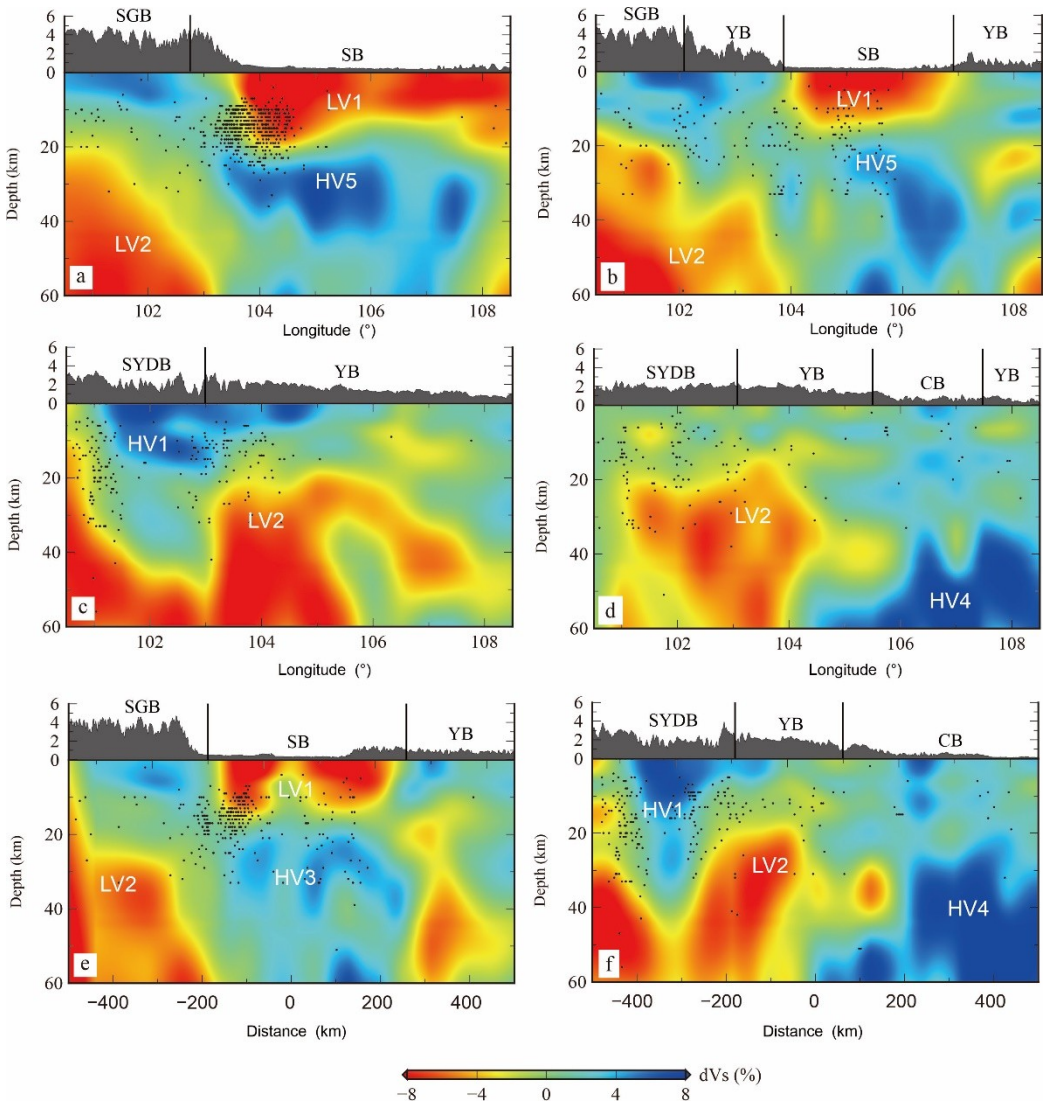

Fig. 8. Vertical cross sections of S-wave velocity. The profile locations are in Fig. 1. SGB: Songpan-Ganzi Block, SB: Sichuan Basin, SYDB: Sichuan-Yunnan diamond-shaped block, YB: Yangtze Block, CB: Cathaysia Block.

We also analysed 6 profiles of S-wave velocity (Fig. 8). The Sichuan Basin (Fig. 8 a and b, HV5) and Cathaysia Block (Fig. 8 d and f, HV4) show high-velocity anomalies at the middle and lower crust. The low-velocity anomaly (LV2) mainly exists in the western part of the study region (Fig. 8 a-f) and

extend to the eastern part locally, or beneath the Yangtze Block (Fig. 8 c, d and f). The seismic activities are mainly distributed at the high-velocity region (Fig. 8 b and d) or the boundary region of the low- and high-velocity (Fig. 8 a, c, e and f).

5. Discussion

The Rayleigh-wave group velocity (9-15s) (Fig. 6 a) and the S-wave velocity at a depth of 10 km show relatively low velocity in the Sichuan Basin (Fig. 7 a). The thickness of the whole sequence of sedimentary layers in Sichuan Basin is about 15 km (Fig. 8 a, b). This is in good agreement with the estimated thickness of continental strata in this basin (Liu et al., 2016). There is a large-scale low-velocity anomaly in the middle-lower crust beneath the Songpan-Ganzi Block and the CYRB, which is consistent with the velocity structure in the Tibet Plateau (Kind et al., 1996). The high-velocity anomaly persists in the central Sichuan Basin within a depth range of about 20-40 km, which may reflect the rigidity crust of this basin (Fig. 7, Fig. 8). Previous studies on surface wave results also indicated that there is a high velocity body at this depth (Yao et al., 2008; Lu et al., 2014). The crustal S-wave velocity structure below 20 km shows low-velocity structure in the western part of the study region (Fig. 8 a-f), whereas eastern part or beneath the

Sichuan Basin is characterized by high-velocity structure (Fig. 8 a and b). Pn wave tomography also demonstrated that there is a low-velocity anomaly beneath the SYDB and the Songpan-Ganzi Block (Lei et al., 2014).

In Fig. 6 and Fig. 7, the low-velocity anomaly (LV2) in the Songpan-Ganzi Block extend to the Yangtze Block, which may imply the extrusion of the Tibet Plateau or the eastward flow in the middle and the lower crust. Wu et al. (1988) obtained 14 terrestrial heat flow data which show high heat flow values in western Yunnan and Panxi areas. Hu et al. (2000) further demonstrated this result based on a new compilation of heat flow data in mainland China. These results suggest melt or partial melt in the crust beneath the Songpan-Ganzi Block and Yangtze Block. Sun et al. (1989) proposed that there are high-conductivity layers in the lower crust and/or upper mantle in western Yunnan and western Sichuan, which are considered to be related to partially molten materials.

As shown in Fig. 8, the seismic activities are mainly distributed at the boundary between the high- and low-velocity structure and the nearby boundary region. This might suggest the ductile deformation of the Songpan-Ganzi Block induced by the eastward extrusion of the Tibet Plateau which is obstructed by the rigid crust of the Sichuan Basin, leading to the stress accumulation and release or the seismic activities.

Although a number of tomographic studies have been carried out in this area and adjacent regions (e.g., Shen et al., 2016; Xie et al., 2013; Chen et al., 2014), our study is the first to define the obvious low-velocity anomaly, which is connected with the channel flow in the crust of the Chuandian region.

6. Conclusions

The results from this study reveal significant difference in the S-wave velocity structure of the crust between the Songpan-Ganzi Block and the Sichuan Basin. The eastward extrusion of the Songpan-Ganzi Block is obstructed by the rigid crust beneath the Sichuan Basin, which might be the cause for stress accumulation and release leading to seismic activities. Our results also indicate that the eastward material flow induced by the extrusion of the Tibet Plateau occurred at this region.

Acknowledgements

We thank the National Key R&D Plan of China (2017YFC601406). Waveform data for this study were provided by the Data Management Centre of China National Seismic Network at the Institute of Geophysics (Zheng et al., 2010). The raw data used in this study can be accessed via

https://doi.org/10.5281/zenodo.4348405.

References

Backus, G., and F. Gilbert (1968), Resolving power of gross earth data, Geophys. *J. R. Astron Soc*., 16, 169-205, doi:10.1111/j.1365-246X.1968.tb00216.x.

Bai, D., X. Ma, J. Weng, X. Kong, M. J. Unsworth, and M. A. Meju (2010), Crustal deformation of the eastern Tibetan plateau revealed by magneto telluric imaging, *Nat. Geo*., 3, 358-362, doi:10.1038/ngeo830.

Bao, X., X. Sun, M. Xu, L. Wang, N. Mi, H. Li, and D. Yu (2015), Two crustal low-velocity channels beneath SE Tibet revealed by joint inversion of Rayleigh wave dispersion and receiver functions, *Earth Planet. Sci. Lett.*, 415, 16-24, doi: 10.1016/j.epsl.2015.01.020.

Bensen, G. D., M. H. Ritzwoller, M. P. Bamin, A. L. Levshin, F. Lin, and M. P. Moschetti (2007), Processing seismic ambient noise data to obtain reliable broad-band surface wave dispersion measurements, *Geophys. J. Int*., 169(3), 1239-1260.

Campillo, M., and A. Paul (2003), Long-Range correlations in the diffuse seismic coda, Science, 299, 547-549, doi: 10.1126/science.1078551.

Chen, M., Huang, H., Yao, H., van der Hilst, R., and F. Niu (2014), Low wave speed zones in the crust beneath SE Tibet revealed by ambient noise

adjoint tomography, *Geophys. Res. Lett.,* 41, 334- 340, doi:10.1002/2013GL058476.

Chen, S., Q. Zheng, and W. Xu (2015), Joint optimal inversion of gravity and seismic data to estimate crustal thickness of the southern section of the north-south seismic belt, *Chin. J. Geophys.,* 58(11), 3941-3951,doi: 10.6038/cjg20151105.

Cotte, N., H. Pedersen, M. Campillo, J. Mars, J. Ni, R. Kind, and E. Sandvol (2010), Determination of the crustal structure in southern Tibet by dispersion and amplitude analysis of Rayleigh waves, *Geophys. J. Int.*, 138(3), 809-819, doi:10.1046/j.1365-246x.1999.00927.x.

De Hoop, M. V., R. D. van der Hilst, and P. Shen, (2006), Wave-equation reflection tomography: annihilators and sensitivity kernels, *Geophys. J. Int.,* 167, 1211-1214, doi:10.1111/j.1365-246X.2006.03132.x.

Deng, Q. D., P. Zhang, Y. Ran, X. Yang, W. Min, and Q. Chu (2002), Basic characteristics of China's active structure, *Sci. China, Ser. D Earth Sci.*, 32(12), 1020-1030, doi:10.3321/j.issn:1006-9267.2002.12.007.

Derode, A. , E. Larose, M. Tanter, de Rosny Julien, and T. Arnaud (2003), Recovering the Green’s function from field-field correlations in an open scattering medium, *J. Acoust. Soc. Am.,* 113(6), 2973-2976, doi:10.1121/1.1570436.

Ditmar, P. G. , and T. B. Yanovskaya (1987), A generalization of the Backus-

Gilbert method for estimation of lateral variations of surface wave velocity, Phys. Solid Earth, *Izvestia Acad. Sci. U.S.S.R.,* 6, 30-60.

Dziewonski, A. M., S. Bloch, and M. Ladinsman, (1969), A technique for the analysis of transient seismic signals, Bull. Seismol. Soc. Am., 59, 427-444.

Fan, L. P., J. Wu, L. Fang, and W. Wang (2015), The characteristic of Rayleigh wave group velocities in the southeastern margin of the Tibetan Plateau and its tectonic implications, *Chin. J. Geophys.*, 58(5), 1555-1567, doi: 10.6038/cjg20150509.

Fang, L. H., J. Wu, Z. Ding, and G. Panza (2010), High resolution Rayleigh wave group velocity tomography in North China from ambient seismic noise, *Geophys. J. Int.*, 181(2), 1171-1182, doi: 10.1111/j.1365-246X.2010.04571.x.

Ferreira, A. M. G., M. Augustin, A. Januka, and F. Michael (2020), Crustal structure of the Azores Archipelago from Rayleigh wave ellipticity data, *Geophys. J. Int.*, doi:10.1093/gji/ggaa076.

Gao, L. J., J. Zhang, and M. Dong (2015), The study of gravity-magnetic anomaly and tectonic background in Sichuan west region, *Chin. J. Geophys.*, 58(8), 2996-3008, doi:10.6038/cjg20150831.

Guo, Z., X. Gao, H. Yao, J. Li, and W. Wang (2009), Midcrustal low-velocity layer beneath the central Himalaya and southern Tibet revealed by ambient noise array tomography, *Geochem. Geophys. Geosyst.,* 10,

Q05007, doi:10.1029/2009GC002458.

Herrmann, R. B., and C. J. Ammon (2004), Surface waves, receiver functions, and crustal structure. Computer Programs in Seismology, Version 3.30.

Herrmann, R. B. (1973), Some aspects of band-pass filtering of surface waves, *Bull. Seismol. Soc. Am.,* 63(2), 663-671.

Hu, H. X., H. Lu, C. Wang, Z. He, and L. Zhu (1986), Explosion investigation of the crustal structure in western Yunnan province, *Chin. J. Geophys*., 29 (02), 133-144.

Hu, J. F., H. Yang, G. Li, H. Peng, and B. José, (2017), Comprehensive crustal structure and seismological evidence for lower crustal flow in the southeastern margin of Tibet revealed by receiver functions, *Gondwana Res.*, 55, 42-59, doi:10.1016/j.gr.2017.11.007.

Hu, S., L. He, and J. Wang (2000), Heat flow in the continental area of China: a new data set, *Earth Planet. Sci. Lett.*, 179(2), 407-419, doi:10.1016/S0012-821X(00)00126-6.

Zeng, S. H., X. Hu, J. Li, S. Xu, H. Fang, and J. Cai, (2015), Detection of the deep crustal structure of the qiangtang terrane using magnetotelluric imaging, *Tectonophysics*, doi:10.1016/j.tecto.2015.08.038.

Huang, J., X. Song, and S. Wang (2003), Fine structure of Pn velocity beneath Sichuan-Yunnan region, *Sci. China, Ser. D Earth Sci.*, 33(Suppl.), 144-150, doi:10.1360/zd2003-33-S1-144.

Jiang, W., J. Zhang, T. Tian, and X. Wang (2012), Crustal structure of Chuan-

Dian region derived from gravity data and its tectonic implications, *Phys. Earth Planet. Inter.*, 212-213, 76-87, doi: 10.1016/j.pepi.2012.07.001.

Kan R. J., S. Zhang, F. Yan, and L. Yu (1977), Present tectonic stress field and its relation to the characteristics of recent tectonic activity in Southwestern China, Chin. J. Geophys., 20(02), 96-109.

Kind, R., J. Ni, W. Zhao, J. Wu, X. Yuan, and L. Zhao (1996), Evidence from earthquake data for a partially molten crustal layer in southern Tibet, *Science*, 274, 1692-1694, doi:10.1126/science.274.5293.1692.

Kirkby, A., and J. Duan (2019), Crustal Structure of the Eastern Arunta Region, Central Australia, From Magnetotelluric, Seismic, and Magnetic Data, *J. Geophys. Res.*, 124(8), doi: 10.1029/2018JB016223.

Lei, J., and D. P. Zhao (2016), Teleseismic P-wave tomography and mantle dynamics beneath eastern Tibet, *Geochem. Geophys. Geosyst.*, 17(5), 1861-1884, doi: 10.1002/2016GC006262.

Lei, J., Y. Li, F. Xie, J. Teng, G. Zhang, C. Sun, and X. Zha (2014), Pn anisotropic tomography and dynamics under eastern Tibetan plateau, *J. Geophys. Res.*,119(3), doi: 10.1002/2013JB010847.

Leveque, J., L. Rivera, and G. Wittlinger (1993), On the use of the checkerboard test to assess the resolution of tomographic inversions, *Geophys. J. Int.*, 115, 313-318, doi: 10.1111/j.1365-246X.1993.tb05605.x.

Levshin, A., L. Ratnikova, and J. Berger (1992), Peculiarities of surface-wave propagation across central Eurasia, *Bull. Seismol. Soc. Am.*, 82(6), 2464-

2493.

Li, P. (1993), Xianshuihe - Xiaojiang fault zone, pp. 81-85, Seismological Press, Beijing.

Li, Y. H., Q. Wu, R. Zhang, J. Pan, R. Zeng and X. B. Tian (2009), Crustal structure in the Yunnan region determined by modeling receiver functions, *Chin. J. Geophys.*, 52(1), 67-80, doi:CNKI:SUN:DQWX.0.2009-01-010.

Li, Y. G., T. L. Henyey, and L.T. Silver (1992), Aspects of the crustal structure of the western Mojave Desert, California, from seismic reflection and gravity data, *J. Geophys. Res.*, 97(B6), doi: 10.1029/91JB02119.

Liu, J. H., F. T. Liu, H. Wu, Q. Li, and G. Hu (1989), Three dimensional velocity images of the crust and upper mantle beneath North-South zone in China, *Chin. J. Geophys.*, 32(02),143-152.

Liu, J. H., H. Wu, and F. Liu, (1996), Features of 3-D velocity distribution and lithosphere structure in south China and its contiguous sea area, *Chin. J. Geophys*., 39(04), 482-492, doi:10.1007/BF02029074.

Liu, S. G., B. Deng, and Y. Zhong (2016), Deep burial of Lower Paleozoic shale gas in Sichuan Basin and its periphery-unique geological effect of strong reform, Earth Science Frontiers, 1, 11-28, doi: 10.13745/j.esf.2016.01.002.

Lu, L. Y., Z. He, Z. Ding, and C. Wang (2014), Azimuth anisotropy and velocity heterogeneity of Yunnan area based on seismic ambient noise, *Chin. J.*

Geophys., 57 (3), 822-836, doi: 10.6038/cjg20140312.

Lin, F. C., M. Ritzwoller, J. Townend, S. Bannister, and M. Savage (2007), Ambient noise Rayleigh wave tomography of New Zealand, *Geophys. J. Int.*, 170(2), 649-666, doi: 10.1111/j.1365-246X.2007.03414.x.

Lobkis, O. I., and R. L. Weaver (2001), On the emergence of the green's function of in the correlations of a diffuse field, *J. Acoust. Soc. Am.,* 110(6), 3011-3017, doi: 10.1016/S0041-624X(02)00156-7.

Pan, J. T., Y. Li, Q. Wu, and Z. Ding (2015), Phase velocity maps of Rayleigh waves in the southeast Tibetan plateau, *Chin. J. Geophys.*, 58(11), 3993-4006, doi: 10.6038/cjg20151109.

Ritzwoller, M. H., and A. L. Levshin (1998), Eurasian surface wave tomography: Group velocity, *J. Geophys. Res.*, 103, 4839-4878, doi:10.1029/97JB02622.

Schubert, G. (2007), Treatise on Geophysics, Treatise on Geophysics .

Shapiro, N. M. , and M. Campillo (2004), Emergence of broadband Rayleigh waves from correlations of the ambient seismic noise, *Geophys. Res. Lett.*, 31 , L07614 , doi : 10.1029/2004GL019491.

Shapiro, N. M., M. Campillo, L. Stehly, and M. H. Ritzwoller (2005) , High resolution surface wave tomography from ambient seismic noise, *Science*, 307, 1615-1618,doi: 10.1126/science.1108339.

518 Shen, C. Y., G. Yang, H. Tan, S. Xuan, and J. Wang (2015), Gravity anomalies
519 and crustal density structure characteristics of profile Weixi-Guiyang,
520 *Chin. J. Geophys.*, 58(11), 3952-3964, doi:10.6038/cjg20151106.
521 Shen, W., M. H. Ritzwoller, D. Kang, Y. Kim, J. Ning, F. C. Lin, W. Wang, Y.
522 Zheng, and L. Zhou (2016) A seismic reference model for the crust and
523 uppermost mantle beneath China from surface wave dispersion,
524 *Geophys. J. Int.*, 206(2), doi:10.1093/gji/ggw175.
525 Su, S. R., Y. Wang and S. Wang (2004), A Study on the Stress Field in the
526 Region of the Lijiang Earthquake, *Geological Review*, 50(1), 57-64,
527 doi:10.3321/j.issn:0371-5736.2004.01.008.
528 Sun, J., and C. Xu (1989), The relationship between the electrical structure of
529 the crust and upper mantle and the tectonic activity in the western
530 Yunnan area, *Seismology and Geology*, 11(001), 35-45,
531 doi:CNKI:SUN:DZDZ.0.1989-01-004.
532 Wang C. Y., J. Wu, H. Lou, X. Wang, F. Wang, and W. Mooney (2002), Three-
533 dimensional velocity structure of crust and upper mantle in Sichuan-
534 Yunnan area, *Acta Seismol. Sinica.*, 24(001), 1-16, doi:
535 10.3321/j.issn:0253-3782.2002.01.001.
536 Wang, F. Y., S. Pan, L. Liu, B. Liu, J. Zhang, X. Deng, and C. Ma (2014), Wide
537 angle seismic exploration of Yuxi-Lincang profile-The research of crustal
538 structure of the red river fault zone and southern Yunnan, *Chin. J.*
539 *Geophys.*, 57(10), 3247-3258, doi:10.6038/cjg20141013.

Wang, W., J. Wu, L. Fang, G. Lai, and Y. Cai (2017), Crustal thickness and Poisson's ratio in southwest China based on data from dense seismic arrays, *J. Geophys. Res*., doi:10.1002/2017JB013978.

Wapenaar, K., D. Draganov, R. Snieder, X. Campman, and A. Verdel (2010), Tutorial on seismic interferometry: Part 1-Basic principles and applications, *Geophysics*, 75(5), A195-A209, doi:10.1190/1.3457445.

Weaver, R. L. (2005), Information from seismic noise, Science, 307, 1568-1569.

Weaver, R. L., and O. I. Lobkis (2001), Ultrasonics without a Source: Thermal fluctuation correlation at MHz Frequencies, *Phys. Rev. Lett*., 87(13), 134301, doi:10.1103/PhysRevLett.87.134301.

Waveform data for this study air provided by Data Management Centre of China National Seismic Network at Institute of Geophysics , China Earthquake Administration.

Wu, J. P., Y. Ming, and C. Wang (2001), The S wave velocity structure beneath digital seismic stations of YUNNAN province inferred from teleseism receiver function modelling, *Chin. J. Geophys.*, 44(02), 228-237, doi: CNKI:SUN:DQWX.0.2001-02-012.

Wu, K. F., J. H. Zu, and Y. Z. Xie (1988), Basic characteristics of geothermal in Yunnan, *Seismology and Geology*, 4, 177-183, doi: CNKI:SUN:DZDZ.0.1988-04-021.

561 Xie, J., M. H. Ritzwoller, W. Shen, Y. Yang, Y. Zheng, and L. Zhou (2013)
562 Crustal radial anisotropy across eastern Tibet and the western Yangtze
563 craton, *J. Geophys. Res.*, 118, 4226-4252, doi:10.1002/jgrb.50296.
564 Xiong, S. B., J. W. Teng, Z. X. Yin, M. H. Lai, and Y. P, Huang (1986),
565 Explosion seismological study of the structure of the crust and upper
566 mantle at southern part of the PanXi tectonic belt, *Chin. J. Geophys.*,
567 29(03), 235-244.
568 Xu, L., R. Stéphane, R. D. V. D. Hilst (2007). Structure of the crust beneath
569 the southeastern Tibetan plateau from teleseismic receiver functions.
570 *Phys. Earth Planet. Inter.,* 165(3-4), 176-193, doi:
571 10.1016/j.pepi.2007.09.002.
572 Xu, Q., J. Zhao, Z. Cui, and M. Liu (2009), Structure of the crust and upper
573 mantle beneath the southeastern Tibetan Plateau by P and S
574 〖JP2〗 receiver functions, *Chin. J. Geophys.*, 52(12), 3001-3008, doi:
575 10.3969/j.issn.0001-5733.2009.12.009.
576 Xu, X. W., X. Wen, R. Zheng, W. Ma, and F. Song (2003), The latest tectonic
577 change patterns and power sources of active blocks in Sichuan-Yunnan
578 area, *Ser. D Earth Sci*., 33(Suppl.),144-150, doi:10.3321/j.issn:1006-
579 9267.2003.z1.017.
580 Xu, Y., X. Yang, and J. Liu (2013), Tomographic study of crustal velocity
581 structures in the Yunnan region southwest China, *Chin. J. Geophys.*,

582 56(6), 1904-1914, doi:10.6038/cjg20130613.
583 Xu, Z. Q., L. Hou, and D. Wang (1990), Thin crust structure and foreland
584 thrust system of the Songpan-Garze Mesozoic collision orogen in
585 southwestern China, *Acta Geosci. Seismol. Sinica*., 11(1), 126-129,
586 doi:CNKI:SUN:DQXB.0.1990-01-034.
587 Yang, Y., M. H. Ritzwoller, A. L. Levshin, and N. M. Shapiro (2007), Ambient
588 noise Rayleigh wave tomography across Europe, *Geophys. J. Int.*, 168,
589 259-274, doi:10.1111/j.1365-246X.2006.03203.x.
590 Yao, H. J., C. Beghein, and R. D. Van der Hilst (2008), Surface wave array
591 tomography in SE Tibet from ambient seismic noise and two-station
592 analysis—II. Crustal and upper-mantle structure, *Geophys. J. Int*., 173(1),
593 205 -219, doi:10.1111/j.1365-246X.2007.03696.x.
594 Yao, H. J., R. D. Van der Hilst, and M. V. de Hoop (2006), Surface-wave array
595 tomography in SE Tibet from ambient seismic noise and two-station
596 analysis—I. Phase velocity maps. *Geophys. J. Int.*,166(2), 732-744, doi:
597 10.1111/j.1365-246X.2006.03028.x.
598 Yanovskaya, T. B., and P. G. Ditmar (1990), Smoothness criteria in surface-
599 wave tomography, *Geophys. J. Int.*, 102, 63-72, doi:10.1111/j.1365-
600 246X.1990.tb00530.x.
601 Zanjani, A., L. Zhu, R. B. Herrmann, Y. Liu, Z. Gu, and J. Conder (2019),
602 Crustal Structure Beneath the Wabash Valley Seismic Zone from the
603 Joint Inversion of Receiver Functions and Surface-Wave Dispersion:

Implications for Continental Rifts and Intraplate Seismicity, *J. Geophys. Res.*, 124(7), doi:10.1029/2018JB016989.

Zhong, D.F. (1998), Paleo-Tethys orogen in western Yunnan and Sichuan, Sciences Press, Beijing, China.

Zhang, F., Q. Wu, Y. Li, R. Zhang, L. Sun, J. Pan, and Z. Ding (2018), Seismic Tomography of Eastern Tibet: Implications for the Tibetan Plateau Growth, *Tectonics*, 37(9-10), 2833-2847, doi:10.1029/2018TC004977.

Zheng D. C., E. Saygin , P. Cummins , Z. Ge , Z. Min , A. Cipta , and R. Yang (2017), Transdimensional Bayesian seismic ambient noise tomography across SE Tibet, *J. Asian Earth Sci*., 53 134, 86-93, doi:10.1016/j.jseaes.2016.11.011.

Zheng, X., C. Zhao, L. Zhou, and S. Zheng (2012), Rayleigh wave tomography from ambient noise in Central and Eastern Chinese mainland, *Chin. J. Geophys.*, 55(6), 1919-1928, doi:10.6038/j.issn.0001-5733.2012.06.013.

Zheng, X., C. Zhao, L. Zhou, and S. Zheng (2015), 3D Shear-Wave Velocity Structure beneath the Southeastern Tibetan Plateau from Ambient Noise, *Bull. Seismol. Soc. Am.*, 105(3), doi:10.1785/0120140211.

Zheng, X. F., Z. Yao, J. Liang, and J. Zheng (2010), The role played and opportunities provided by IGP DMC of China National Seismic Network in Wenchuan earthquake disaster relief and researches, *Bull. Seismol. Soc.*

Am., 100(5B), 2866-2872, doi:10.1785/0120090257 .

Zhou, L. Q., J. Xie, W. Shen, and Y. Zheng (2012), The structure of the crust and uppermost mantle beneath South China from ambient noise and earthquake tomography, *Geophys. J. Int.*, 189(3), doi:10.1111/j.1365-246X.2012.05423.x.